Operating Characteristics of a 60- and 10-cm Electric Arc-Driven Shock Tube—Part I: The Driver

Surendra P. Sharma* and Chul Park*
NASA Ames Research Center, Moffett Field, California 94035

This is the first part of a two-part paper describing the operating characteristics of the electric arc-driven shock-tube facility at NASA Ames Research Center. In this part, the operating envelope of the facility and the technology of the arc driver are presented. Specifically, the question as to how well the behavior of the arc driver is understood and controlled is addressed. A plasma kinetics model of the exploding wire is developed to describe the arc behavior in the driver. Using this model, the performance parameters for the arc driver, and thereby the performance of the facility, can be predicted approximately.

Nomenclature

A_d = cross-sectional area of driver, m^2
A_w = characteristic constant of the metal
a = speed of sound
C = capacitor bank capacitance, F
C_e = mean thermal velocity of electrons, $\sqrt{8kT_e/\pi m_e}$
C_v = specific heat of trigger wire
D = diameter of the driver
D_a = diameter of the arc column
E = electric field intensity, V/m
E_I = ionization potential
e = electronic charge
Gr = Grashoff number, $\rho^2 g \Delta T D^3/(\mu T)$
g = Earth gravitational acceleration
I = total current, A
I_a = arc current, A
I_w = current in trigger wire, A
j_e = electric current density in gas phase, A/m^2
j_t = electric current density due to thermionic emission, A/m^2
K_f = forward (dissociation or ionization) rate coefficient, $cm^3\ mole^{-1}\ s^{-1}$
K_r = recombination rate coefficient, $cm^6\ mole^{-2}\ s^{-1}$
k = Boltzmann constant
L_a = arc inductance, H
L_x = external inductance, H
m_e = electron mass
m_w = mass of trigger wire
Nu = Nusselt number
n_a = number density of neutral atoms, m^{-3}
n_e = electron number density, m^{-3}
P = gas pressure
Pr = Prandtl number
q = heat transfer rate, J/m s
R_a = arc resistance, Ω
R_w = resistance of trigger wire, Ω
R_x = external resistance, Ω
T = gas temperature, K
T_e = electron temperature, K
T_w = trigger wire temperature, K
V_a = arc volume, m^3
V_d = driver volume, m^3
α = degree of ionization or dissociation
ϵ = internal energy of the gas per unit mass
ϵ_w = internal energy of the trigger wire per unit mass
γ = specific heat ratio
χ_w = work function of trigger wire
κ = thermal conductivity
μ = viscosity
ν_{es} = collision frequency of electrons for collisions with species "s", s^{-1}
ρ = gas density, kg/m^3
σ = plasma conductivity, mho/m

Subscripts

a = arc
e = electron
s = shock layer
t = thermionic emission
w = driver trigger wire
x = external
1 = initial driven-tube condition
2 = behind the primary shock
4 = initial driver condition
5 = reflected shock
∞ = test section

I. Introduction

In recent years, interest has been aroused to understand the nature and effects of high-temperature real-gas phenomena occurring in the flow around hypersonic vehicles. At flight Mach numbers above about seven, portions of the airflow around a vehicle are sufficiently hot to produce vibrational relaxation, dissociation, and even ionization. The heat-transfer measurements conducted on the surface of the heat-shield tiles of the Space Shuttle demonstrated that the airflow around the vehicle is substantially dissociated, and that the heat-transfer rate to the surface can be reduced by using a material noncatalytic to dissociated species. The impact of such real-gas effects on aerodynamic forces such as lift, drag, and moments is not yet clear. However, there is at least some reasonable basis to suspect that the real-gas effect is responsible for the anomalous pitching moment encountered during the entry flight of the Apollo[1] and the Space Shuttle vehicles.[2]

Motivated by such interests, considerable effort has been expended in recent years to numerically compute the real-gas

Presented as Paper 88-0142 at the AIAA 26th Aerospace Sciences Meeting, Reno, NV, Jan. 11-14, 1988; received March 10, 1988; revision received Oct. 5, 1989.

*Research Scientist. Associate Fellow AIAA.

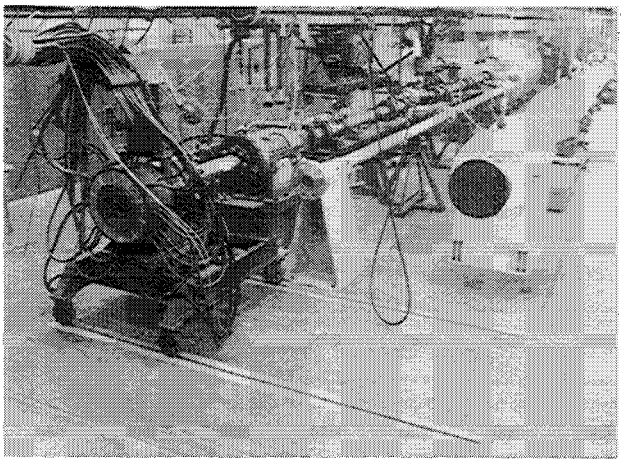

Fig. 1 NASA Ames 60- and 10-cm electric arc-driven shock-tube facility. The tube at the center is the temporary setup for testing the aluminum driven tube.

flows around a vehicle. Accuracy of such calculations is as yet virtually unknown. Unlike for the perfect gas, there are still many physical constants that are unknown for high-temperature real gases, even though a great deal has been found through theoretical computations.[3,4] Thermochemical models describing the phenomena and the numerical algorithms used for the computation also contain many uncertainties. For these reasons, it becomes desirable to conduct an experiment. Such experiments can provide the needed physical constants and verify the validity of the thermochemical models and the computational algorithms used.

The question of how to simulate the real-gas flows and how to diagnose them has been addressed in a recent paper by the present authors.[5] The paper points out, among others, that to meet the current and expected future needs it is necessary to 1) test low-density nonequilibrium flows in suborbital to superorbital velocities, and 2) produce high-enthalpy flows in chemical equilibrium in the test section of a hypersonic wind tunnel. Usefulness of various experimental facilities on these two fields of application is discussed in the earlier paper. The present two-part paper is a sequel to that paper and focuses on the usefulness of an electric arc-drive shock-tube facility toward these goals. One such facility has been in existence since the 1960s at NASA Ames Research Center. The operating characteristics of the facility charted during the initial phase of its operation are described in detail by Reller,[6] but the preceding two issues were not addressed therein.

In part I of this paper, we present the envelopes of operational performance of the facility and the status of the technology of the arc driver that controls the performance. The arc-driver technology is based on the numerical predictive capability developed recently, with which the behavior of the arc is calculated using the plasma kinetic theory for an exploding wire.

II. Performance Envelopes

Shock tubes are unique in producing homogeneous high-temperature gas samples heated to an enthalpy and pressure calculable and selectable from the state of the undisturbed gas and measured shock velocity. In order to study the high-temperature phenomena accompanying hypersonic flights, the speed of the primary shock wave must be large. The shock speed is dictated mostly by the speed of sound of the driver gas a_4. For an infinitely large pressure ratio (the ratio between the pressure of the driver gas to the pressure of the driven gas), the shock speed U_s is determined by[7]

$$U_s = \frac{a_4}{\gamma_4 - 1}$$

where γ_4 is the ratio of specific heats. To increase a_4, one can reduce the molecular weight by using a light gas such as hydrogen or helium and raising the temperature of the driver gas by heating. The commonly used methods of heating are 1) warming the gas using an electrical heater[8]; 2) combustion of hydrogen with oxygen, diluted by either hydrogen or helium[9]; 3) adiabatically compressing hydrogen or helium using a piston[10]; and 4) by discharging an electrical current through the driver gas.[11-15] There is an extraordinary method of producing extremely high shock speeds using high explosives,[16] but this method destroys almost all hardware in each run and cannot be considered in a laboratory facility.

In the first method, the maximum temperature of the driver gas is limited to about 700 K. In the second method, the gas temperature can reach about 2500 K. But the oxygen in the driver gas needed for the combustion raises the average molecular weight. In the third method, one can heat either pure hydrogen or helium driver gas to nearly 3000 K, thus producing a stronger shock than the first two methods. The piston compression occurs over a relatively long period of time (several hundred milliseconds), and therefore, at temperatures above 3000 K, the materials of the driver tube and the piston begin to melt and ablate. In the fourth method, electrical discharge heats either hydrogen or helium to a temperature of about 8000 K for hydrogen and about 20,000 K for helium without causing melting or ablation of the materials, because the discharge time is very short. The maximum temperatures are set by the onset of ionization and accompanying energy loss by radiation. Thus, an electrical arc-driven shock tube operating on this principle produces the highest shock speed.

The electric arc-driven shock-tube facility at NASA Ames Research Center consists of one driver system and two parallel driven tubes. One is a 10-cm i.d. tube 12 m in length, and the other is a 60-cm i.d. tube 21 m in length, both made of stainless steel (Fig. 1). The driver can be operated in two configurations: 1) a 17.7-cm conical drive configuration with a 10.16-cm exit (driver volume = 632 cm^3), and 2) a variable length (34–137 cm) 10-cm i.d. cylindrical configuration (driver volume = 2669–10,752 cm^3). The length of the cylindrical drivers can be varied by using a Lexan filler plug. A schematic of the cylindrical driver is shown in Fig. 2. The current collector ring consists of two coaxial copper cylinders. The outer cylinder flanged to the driver tube is electrically grounded, whereas the inner cylinder is connected by a copper spring contact plate to the main electrode. The high-voltage electrode has a hollow core through which a rod extends back to the piston of a pneumatic solenoid. The solenoid actuates the trigger. Several different materials have been used for the trigger wire, but most of the tests have been made with tungsten wire. The trigger wire is extended along the length of the arc chamber to the ground plate (Fig. 2). When the slack wire is drawn to the high-voltage electrode, the current flow is initiated. The thermionic emission from the trigger wire helps ignite the discharge.[17-19]

Energy to the driver is supplied by a 1.24-MJ, 40-kV capacitor energy-storage system. The six-tier capacitor bank has 220 capacitors. By using different combinations of series-parallel connections, the capacitance of the bank can be varied from 149 μF to its maximum value of 6126 μF (1530 μF for 40-kV operation). Nominal total system inductance exclusive of the load (arc) is 0.26 μH, and the resistance is 1.6 mΩ.

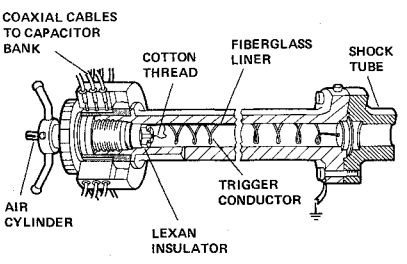

Fig. 2 Schematic of the cylindrical driver.

Current waveforms are recorded during each discharge. The shock velocity is computed by recording the time of shock arrival at various locations along the length of the tube, using conductivity probes and digital counters.

Using the two different driven tubes, by varying the driver/driven gas combination, driver charge pressure, and preset capacitor bank voltages, shock velocities in the range of 3.0–50.0 km/s have been obtained. The following is a list of the ranges of operating conditions:

1) Driver charge pressure: 1.0–27.2 atm
2) Driven tube initial pressure:
   (i) 60 cm tube: 0.01–10 Torr
   (ii) 10 cm tube: 0.1–760 Torr
3) Driver gas: H_2, He, N_2, H_2/Ne
4) Driven gas: Air, H_2, O_2, Ne, K_r
5) Capacitor bank:
   (i) Voltage: 16.0–38.0 kV
   (ii) Capacitance: 149–6126 μF

The diaphragm is made of mylar 0.35–0.50 mm in thickness. It is ruptured due to the rise in pressure within the driver during the capacitor discharge. There is a time lag of 20–40 μs between the instant the breaking pressure is reached (approximately 11.5 atm for a 0.35 mm diaphragm), and the instant the diaphragm is fully open.

A total of 760 runs have been made to date. Of these, 75 runs are shown in Fig. 3. These runs can be classified into three different categories: 1) air or a gas of similar molecular weight (argon, carbon dioxide) as the test gas in the 10-cm tube, 2) air or a gas of similar molecular weight as the test gas in the 60-cm tube, and 3) hydrogen as the test gas in the 10-cm tube. These three classes of operations occupy different regions in the velocity-pressure plot in Fig. 3.

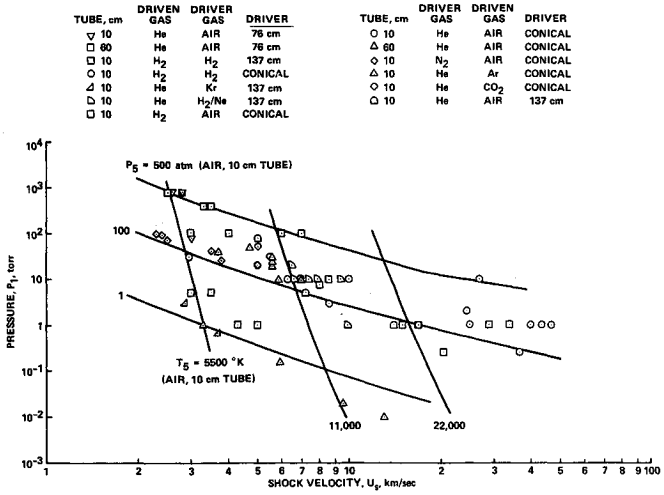

Fig. 3 Measured shock velocity vs initial driven-tube charging pressure P_1.

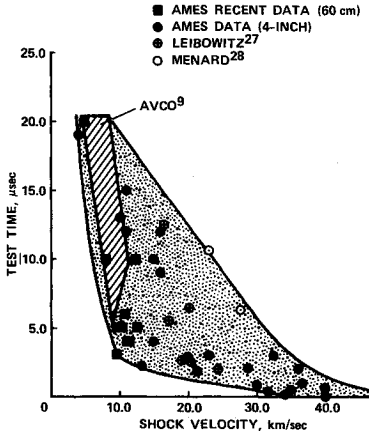

Fig. 4 Measured test times in air vs shock velocity in the NASA Ames facility compared with those in other facilities.[3–5]

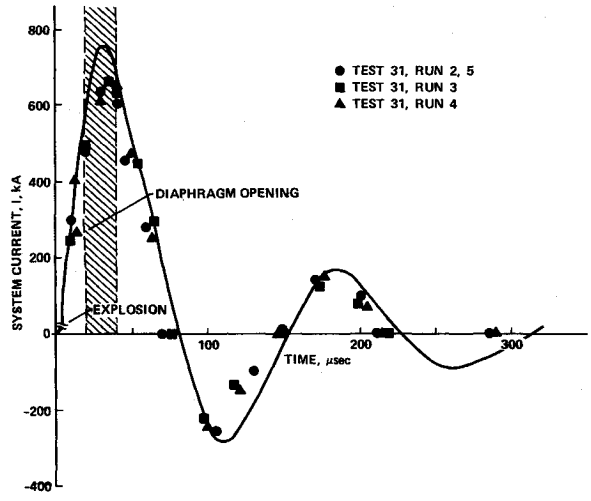

Fig. 5 The time record of electrical current through the driver discharge system compared with the theoretical calculation, with the conical driver, nitrogen as the driver gas, with capacitor setting of capacitance C = 861.3 μF, voltage = 23 kV, (charging energy = 223 kJ), external inductance L_x = 0.212 μH, and external resistance Re = 1.6 mΩ.

Air runs in the 10-cm tube were made mostly at high charging pressures and were made for hitherto unpublished purposes connected with national defense. Some of the runs in the 10-cm tube with a heavy (not hydrogen) gas have been made also for the study of gasdynamic lasers[20] and for the purpose of studying radiation characteristics of the flow around an entry vehicle known as the Galilleo Probe, which will enter the atmosphere of the planet Jupiter.[21] The runs in the 60-cm tube were made mostly for the Galileo Probe. All of these runs have been made with the driven-tube charging pressure of few Torrs or higher. The hydrogen runs in the 10-cm tube were made at around 1 Torr, and were for the purpose of studying the radiative characteristics of the gas in the flow regime expected also of the Galileo Probe. As seen in the figure, the hydrogen runs produced shock speeds of up to about 50 km/s. At such high speeds, the pressure behind the primary shock was of the order of few atmospheres. Therefore, except in the region immediately behind the shock (for about 0.5 μs), the hydrogen flow tended to be in equilibrium. Test times recorded for shock-tube runs in air using various drivers and driver gases are shown in Fig. 4. As seen in the figure, the facility produces test times that are at least comparable to those obtained elsewhere.[11,14,22]

Most previous test runs in the facility were made with a driven-tube charging pressure that produced an equilibrium or near-equilibrium condition behind the primary shock. As mentioned in the Introduction, there is a need for producing low-density nonequilibrium flows. For this reason, tests have been made in the recent months with low charging pressures, that is, with P_1 values between 0.01 and 1 Torr, in both the 10-cm and 60-cm tubes, producing shock velocities in the range of 5–15 km/s.

III. Arc Driver

Figure 5 shows records of the electric current during a discharge for three runs. As the figure shows, current rises at first with a steep gradient for about 40 μs, falls and reverses, and reverses again and again. That is, the system rings. During the period of negative current, the electrodes of the capacitor are exposed to a negative voltage. The diaphragm begins to open at around 20-μs and is fully open at around 50-μs. Thus, even after the diaphragm is open, the electric discharge continues. Time-dependent calculation of the shock-tube flow shows

that the electric discharge after the diaphragm opening contributes very little to raising the velocity of the primary shock wave in the driven section. Therefore, for an efficient use of the driver system, the electric energy should be deposited into the gas with a steepest possible rise time, before the diaphragm opens.

In a capacitor storage system of this type, the current rise time strongly depends on the impedance of the gaseous discharge column in the driver. The impedance is determined in turn by the driver dimensions and driver gas parameters such as the type of gas (atom or molecule), density, charging pressure, ionization potential, or the specific heat.

Understanding the electric discharge characteristics of the driver is important for two reasons. First, in order to produce a new driven-gas condition not produced in the past, one would like to know how to configure the capacitor banks and what voltage to charge the system. To select these parameters, the relationship between the gas properties and the electrical discharge characteristics must be known. Second, one would like to minimize the negative voltage on the capacitors, because usually the insulation in the capacitors between the two electrodes tends to be weakened by the application of high negative voltages.

Efforts have been made in the past to understand the discharge phenomenon theoretically. References 12 and 15 show how the knowledge gained by such efforts contributes to improving the performance of the facility. However, the past efforts have concentrated mostly on the electric characteristics external to the arc discharge. For this reason, a theoretical model is developed in the present work utilizing plasma kinetics theory to characterize the behavior of the arc discharge in the driver. The driver gas is assumed to be helium, the most frequently used gas. The electric discharge is envisioned to occur in the following two phases.

Pre-Explosion (Phase 1) Period

Prior to the explosion and vaporization of the trigger wire, named the phase 1 period, electrical current passes mostly through the trigger wire. Temperature of the trigger wire rises by ohmic heating. Defining ϵ_w as the internal energy of the wire, I_w as the current through the wire, and R_w as the resistance of the wire, the temperature rise is described by

$$\frac{d\epsilon_w}{dt} = I_w^2 R_w \tag{1}$$

where $\epsilon_w = m_w c_v T_w$. This Joule heat is eventually transferred into the gas. The temperature rise in the gas due to this heating causes ionization of the gas, turning the gas into a plasma, and thereby allowing a portion of the electrical current to pass through the plasma. The internal energy of the gas $\epsilon = (3/2)(1+\alpha)RT + E_I\alpha$ obeying the equation

$$\frac{d}{dt}(\rho\epsilon) = j_e E + \frac{I_w^2 R_w}{V_d} \tag{2}$$

The electrical field strength E is related to the current via the Ohmic law applied to the trigger wire, as $E = I_w R_w / l$, where l is the length of the trigger wire. The current through the trigger wire can be expressed in terms of the total system current I as $I_w = (I - A_d j_e)$.

Ionization of the gas is caused first by the *boiling* of free electrons from the surface material in a process called thermionic emission. It is customary to characterize this phenomenon in terms of the thermionic emission current density j_{t0} given by[22]

$$j_{t0} = A_w T_w^2 \exp\left(-\frac{\chi_w}{kT_w}\right)$$

In the presence of a strong electrostatic field, the number of electrons drawn out of the metal surface further increases. This intensification of the thermionic emission phenomenon due to an electric field is called the Schottky effect. The resulting current is given by[23]

$$j_t = j_{t0} \exp\left(\frac{0.4389\sqrt{E}}{T_w}\right)$$

The density of the electrons produced by these thermionic phenomena n_{et} can be calculated from the relation $j_t = e n_{et} C_e$. The rate of change of the electron density produced by the thermionic emission can be written as

$$\frac{dn_{et}}{dt} = \frac{1}{eC_e}\frac{dj_t}{dt}$$

Once electrons are produced by the thermionic processes, they produce more electrons through the gas-phase collisional ionization process, provided the (electron) temperature is sufficiently high, and are removed partly by the collisional recombination process. Therefore, the rate of change of electron density is a sum of that due to the thermionic emission and that due to the gas phase reactions in the form

$$\frac{dn_e}{dt} = \frac{1}{eC_e}\frac{dj_t}{dt} + K_f n_a n_e - K_r n_e^3 \tag{3}$$

The recombination rate coefficient for helium is obtained from Ref. 24, and the ionization rate is deduced from the recombination rate through the use of the detailed balance relationship (Saha equation).

The electron temperature T_e appearing in Eqs. (1-3) is governed by the electron energy conservation equation[25]

$$\frac{d}{dt}\left(\frac{3}{2}kn_e T_e\right) = j_e E - \frac{3}{2}kn_e \sum_s \frac{2m_e}{m_s}\nu_{es}(T_e - T) - E_I\frac{dn_e}{dt} \tag{4}$$

The collision frequency for the positive ion is given in terms of the well-known Coulomb cross section.[25] It is also well known for the neutral helium atoms.[26] Neglecting the mobility of ions, the current through the plasma is assumed to be due to the motion of electrons. The electron current density j_e is in turn governed by the electron momentum equation

$$\frac{dj_e}{dt} = \frac{n_e e^2}{m_e} E - j_e \sum_s \nu_{es} \tag{5}$$

The total current I in turn is governed by the equation of its conservation (Fig. 6)

$$L_x\frac{d^2I}{dt^2} + R_x\frac{dI}{dt} + L_x\frac{I}{C} + R_w\left(\frac{dI}{dt} - A_d\frac{dj_e}{dt}\right) + (I - j_e A_d)\frac{dR_w}{dt} = 0 \tag{6}$$

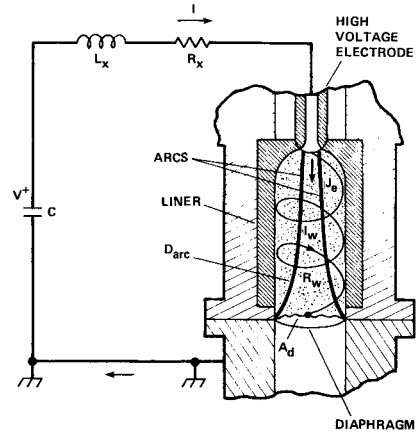

Fig. 6 Schematic of the exploding wire and plasma heating in the driver.

These six ordinary differential equations, augmented by the equation of state and the relationship between the wire resistance R_w and the wire temperature T_w, completely specify the evolution of the properties during the first phase. The six unknowns are n_e, T_e, j_e, T, T_w, and I.

The final values of the plasma parameters at the point of explosion, as computed in this period, are used as the initial conditions for the next postexplosion period.

Postexplosion (Phase 2) Period

At the beginning of this phase, it is assumed that the trigger wire has exploded and vaporized instantly. As the initial conditions show that the plasma is highly conducting, an arc forms as a result. The phenomena of arc formation is a complicated process and is not very well understood. It is widely believed that an arc is initiated by the overheating of electrodes and consequent onset of thermionic emission from the electrode material. The arc current is thought to be dependent on the electrode geometry, ionization potential of the discharge gas, and the gas pressure. For simplicity, in the present model the following empirical relationship for the arc current has been assumed[27]

$$I_a = \left[\frac{E}{1.66 \times 10^4} P^{-0.2}\right]^{-1.35} \tag{7}$$

where P is the pressure in atm. The arc is considered to have a cylindrical shape with a diameter D_a, so that the current through the arc becomes $I_a = (\pi D_a^2/4) j_{ea}$, where j_{ea} is the current density in the arc column. Since the arc conductivity is very high, the increase in conductivity due to the vaporized trigger wire material is neglected.

Since both the arc region and the surrounding gas are plasma in nature, gas-phase conservation equations similar to those in the first phase separately govern the properties of both these regions. The rate of change of the electron number density in the surrounding plasma is given by

$$\frac{dn_e}{dt} = K_f n_a n_e - K_r n_e^3 \tag{8}$$

Electron energy equation and momentum equation for the surrounding plasma are written as

$$\frac{d}{dt}\left(\frac{3}{2} k n_e T_e\right) = j_e E - \frac{3}{2} k n_e \sum_s \frac{2m_e}{m_s} \nu_{es}(T_e - T) - E_I \frac{dn_e}{dt} \tag{9}$$

$$\frac{dj_e}{dt} = \frac{n_e e^2}{m_e} E - j_e \sum_s \nu_{es} \tag{10}$$

Three equations identical to Eqs. (8–10) are written for the arc column.

In writing the total energy equations for this period, it is necessary to account for the heat transfer from the arc to the surrounding plasma, because, unlike in the first phase, the diameter of the arc is fairly large and so the heat transfer is not instant. The heat transfer from the arc column to the surrounding gas occurs mostly via the convection due to buoyancy and can be written in the form

$$q = \kappa Nu \pi (T - T_a)$$

The Nusselt number for this buoyancy-controlled case can be determined in turn assuming the arc column to be a horizontal cylinder, leading to[27]

$$Nu = 0.53 \left[\mathrm{Gr} \frac{Pr^2}{0.953 + Pr}\right]^{0.25}$$

The Prandtl number is taken to be 0.7. The losses due to the radiation from the arc column are negligible. The rate of change of the internal energy within the arc can now be written as (Fig. 6)

$$\frac{d}{dt}\left(\frac{\pi D_a^2}{4} \rho \epsilon_a\right) = I_a E - q \tag{11}$$

The rate of change of the internal energy in the surrounding gas becomes

$$\frac{d}{dt}\left(\frac{\pi D^2 - \pi D_a^2}{4} \rho \epsilon\right) = \frac{\pi D^2 - D_a^2}{4} \rho \epsilon_a j_e E + q \tag{12}$$

The arc diameter D_a and the arc voltage E are determined from the dependent variable in Eq. (7) and from the current and current density relationship. The internal energy of the gas ϵ is determined as in phase 1.

The total current is expressible now as

$$I = I_a + j_e A_d$$

Since most of the electric current passes through the arc, one can approximate the second derivative of I as

$$\frac{d^2 I}{dt^2} \approx \frac{d^2 I_a}{dt^2}$$

Using this approximation, the conservation of electrical current can be written as (Fig. 6)

$$(L_x + L_a)\frac{d^2 I}{dt^2} + R_x \frac{dI}{dt} + \frac{I}{C} + R_a \frac{dI_a}{dt} + I_a \frac{dR_a}{dt} = 0 \tag{13}$$

where $R_a = 1.0/(\pi D_a^2 \sigma_a / 4l)$, with σ_a as the arc conductivity calculable from well-known expressions.[20] The arc inductance is determined by $L_a = 1.0 \times 10^{-7} [0.5 + \log_{10}(D/D_a)]$. There

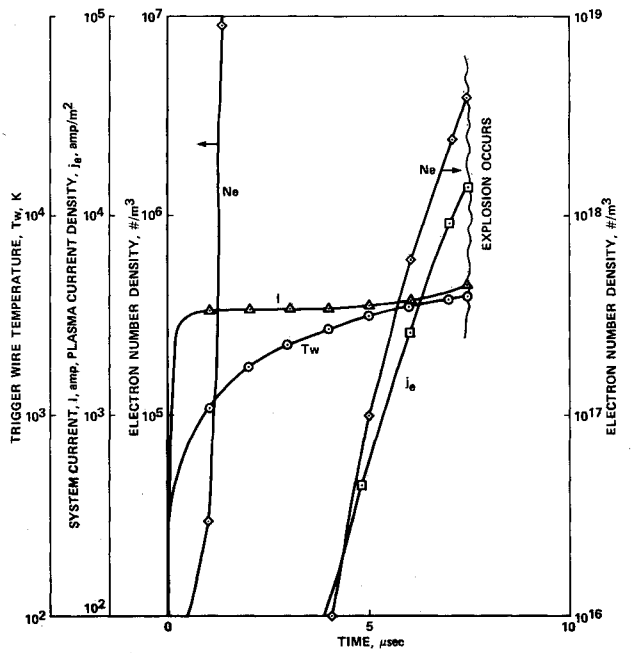

Fig. 7 Computed electrical and plasma parameters for the conical driver for the period before the explosion of the wire (phase 1), with helium as the driver gas at a pressure of 9.2 atm. The trigger wire is made of tungsten, 0.25 mm in diameter and 0.33 m in length.

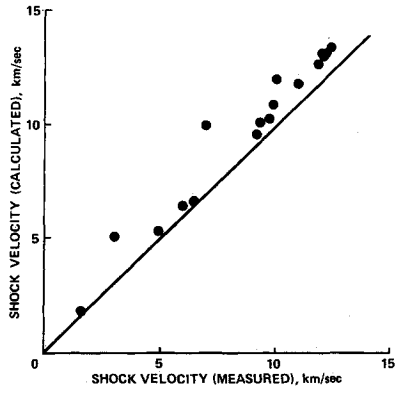

Fig. 8 Comparison between the measured shock velocities and the shock velocities calculated using the present plasma kinetic theory for the driver heating, with helium as the driver gas.

are now two sets of four differential equations describing the plasma properties for both the arc and the surrounding region with two sets of unknowns: electron number density, electron temperature, current density, and gas temperature. One additional equation [Eq. (13)], describing the total electrical current, makes a total of nine ordinary differential equations with nine unknowns: n_e, T_e, j_e, T, n_{ea}, T_{ea}, j_{ea}, T_a, and I. The results of the calculation in the first phase are used as the initial conditions for the calculation for the second phase.

These resulting differential equations are found to be numerically very stiff. These equations are integrated using the stiff equation solver DGEAR[28] in the International Mathematics and Statistics Library (IMSL).[29] Figure 7 shows the computed electrical parameters during the first phase. As the figure shows, the system current I rises rapidly during the first 0.1 μs to a value of 3.67 kA and remains constant until the trigger wire explodes. This value is about 0.5% of the peak current achieved in the second phase (Fig. 5). This period of low constant current is referred to commonly as the *dwell time* and has been widely observed in the experiments. During the first 2.5 μs of the first phase, an electron avalanche occurs and the electron number density increases from almost zero to $\sim 10^{13}$ m^{-3}. Then the increase in the electron number density slows down, but the plasma current density still keeps growing at an ever so fast rate, reaching a value of $\sim 10^4$ A m^{-2} at $t = 7.0$ μs. At $t = 7.4$ μs, the temperature of the trigger wire reaches 4000 K and the wire explodes and vaporizes. By this time, the gas temperature has reached 8000 K. This concludes the first phase.

In the second phase an arc is initiated and a major portion of the current is drawn by the arc. A typical solution for the second phase current is shown in Fig. 5 (solid curve). The solution is obtained for the 0.177-m conical driver with the bank capacitance of 861.3 μF, bank voltage of 23,000 V, and the driver gas pressure of 9.2 atm. The computed values have been found to be in close agreement with the experimental results (symbols).

Once the arc current and voltage transients in the driver are computed, using the energy input, a one-dimensional gasdynamics code is used to compute the shock velocity in the driven section. Figure 8 compares the computed and measured shock velocities. The computed results seem about 7% higher than the experimental results.

The present calculation techniques enable us to select proper driver operational parameters and predict the shock-tube performance. Presently, using the constructed model, design of an electric arc driver, with an energy capacity higher than the present driver, is being considered.

IV. Conclusions

The plasma kinetic model considers the plasma heating in the arc driver to occur in two phases: 1) pre-explosion, and 2) postexplosion periods. The pre-explosion period lasts typically for 7–10 μs and is primarily responsible for the production of electrons, thereby increasing the plasma conductivity. The gas temperature is also increased to 8000–10,000 K. During the postexplosion period, the plasma draws high currents ($\sim 8 \times 10^5$ A), and the plasma heating process speeds up. Because of the plasma and external impedance, current oscillations typical to LCR circuits are observed. The one-dimensional code using the electrical data from the plasma kinetics model predicts about 7% higher velocities than that recorded during actual experiments. The production of radial shock waves in the driver should be taken into account in future models for better agreement between theory and experiments.

References

[1]Park, C., and Yoon, S., "Calculation of Real-Gas Effects on Blunt-Body Trim Angles," AIAA Paper 89-0685, Jan. 1989.

[2]Stalker, R. J., "An Appreciation of Some Nonequilibrium Effects in Hypervelocity Aerodynamics," AIAA Paper 88-0459, Jan. 1988.

[3]Cooper, D. M., Jaffe, R. L., and Arnold, J. O., "Computational Chemistry and Aeroassisted Orbital Transfer Vehicles," *Journal of Spacecraft and Rockets,* Vol. 22, No. 1, 1985, pp. 60–67.

[4]Sharma, S. P., Huo, W. M., and Park, C., "The Rate Parameters for Coupled Vibration Dissociation in a Generalized SSH Approximation," AIAA Paper 88-2714, June 1988.

[5]Sharma, S. P., and Park, C., "A Survey of Simulation and Diagnostic Techniques for Hypersonic Nonequilibrium Flows," AIAA Paper 87-0406, Jan. 1987.

[6]Reller, Jr., J. O., "Design and Performance of the Ames Electric-Arc Shock Tunnel," NASA TM-X-2814, June 1963.

[7]Glass, I. I., and Patterson, G. N., "A Theoretical and Experimental Study of Shock-Tube Flows," *Journal of the Aeronautical Sciences,* Vol. 22, No. 2, 1955, pp. 73–100.

[8]Wittliff, C. E., "Hypersonic Shock Tunnel Heat-Transfer Tests of the Space Shuttle SILTS Pod Configuration," AIAA Paper 83-1535, June 1983.

[9]Hiers, R. S., Loubsky, W. J., and Stewart, D. A., "Performance of a Combustion-Driven Shock Tunnel with Application to the Tailored-Interface Operating Conditions," NASA TM-X-54960, Dec. 1964.

[10]Stalker, R. J., and Hornung, H. G., "Two Developments with Free Piston Drivers," *Shock Tubes Proceedings of the 7th International Shock-Tube Symposium,* edited by I. I. Glass, Univ. of Toronto, Toronto, Ontario, Canada, 1970, pp. 242–258.

[11]Camm, J. C., and Rose, P. H., "Electric Shock Tube for High Velocity Simulation," AVCO Everett Research Lab., Research Rept. 136, July 1962.

[12]Dannenberg, R. E., "Development of Dynamic Discharge Arc Driver with Computer-Aided Circuit Simulation," *AIAA Journal,* Vol. 14, No. 9, 1976, pp. 1183–1188.

[13]Dannenberg, R. E., "A New Look at Performance Capabilities of Arc-Driven Shock Tubes," *Shock Tube and Shock Wave Research: Proceedings of the 11th International Symposium on Shock Tubes and Shock Waves,* edited by B. Ahlborn, A. Herzberg, and D. Russell, Univ. Washington Press, Seattle, WA, 1978, pp. 416–431.

[14]Menard, W. A., "A Higher Performance Electric-Arc-Driven Shock Tube," *JPL Quarterly Technical Review,* Vol. 1, No. 1, 1971, pp. 17–28.

[15]Dannenberg, R. E., "GAIM—Gas-Addition, Impedance-Matched Arc Driver," *Shock Tubes and Waves: Proceedings of the 12th International Symposium on Shock Tubes and Waves,* edited by A. Lifshitz and J. Rom, Magnes, Hebrew University, Jerusalem, 1980, pp. 599–606.

[16]Compton, D. L., and Cooper, D. M., "Duplication in a Shock Tube of Stagnation Region Conditions on a Jovian Atmosphere-Entry Probe," *Recent Developments in Shock Tube Research: Proceedings of the 9th International Shock-Tubes Symposium,* edited by D. Bershader and W. Griffith, Stanford Univ., Stanford, CA, 1973, pp. 318–329.

[17]Dannenberg, R. E., and Silva, A. F., "Arc Driver Operation for Either Efficient Energy Transfer or High-Current Generation," *AIAA Journal,* Vol. 10, No. 12, 1972, pp. 1563–1564.

[18]Dannenberg, R. E., and Silva, A. F., "Exploding Wire Initiation and Electrical Operation of a 4-kV System for Arc-Heated Drivers up to 10-ft Long," NASA TN-D-5126, April 1969.

[19]Dannenberg, R. E., "A Conical Arc Driver for High-Energy Test Facilities," *AIAA Journal,* Vol. 10, No. 12, 1972, pp. 1692–1694.

[20]McKenzie, R. L., "Diatomic Gasdynamic Lasers," *Physics of Fluids,* Vol. 15, No. 12, 1972, pp. 2163–2173.

[21]Shirai, H. and Park, C., "Experimental Studies of Radiative Base Heating of a Jovian Entry Model," *Progress in Astronautics and Aeronautics: Entry Heating and Thermal Protection,* Vol. 69, edited by W. B. Olstad, AIAA, New York, 1980, pp. 148–171.

[22]Leibowitz, L. P., "Attainments of Jupiter Entry Shock Velocities," *AIAA Journal,* Vol. 13, No. 3, 1975, pp. 403–404.

[23]Cobine, J. D., *Gaseous Conductors,* McGraw-Hill, New York, 1941, Chaps. 5 and 9.

[24]Minnov, E. H., and Hirschberg, J. G., "Electron-Ion Recombination in Dense Plasmas," *Physical Review,* Vol. 125, No. 3, 1962, pp. 795–801.

[25]Sutton, G. W. and Sherman, A., *Engineering Magnetohydrodynamics,* McGraw-Hill, New York, 1965.

[26]Delcroix, J. L., *Plasma Physics, Vol. 2, Weakly Ionized Gases,* Wiley, London, 1968.

[27]Eckert, E. R. G., and Drake, R. M., Jr., *Heat Transfer,* McGraw-Hill, New York, 1959, Chap. 11.

[28]Hindmarsh, A. C., "Gear: Ordinary Differential Equation System Solver," Lawrence Livermore Lab., Rept. UCID-30001, Rev. 3, Dec. 1974.

[29]International Mathematics and Statistics Library, IMSL, Inc., Houston, TX, June 1982.